THE EVOLUTION OF SOOT MORPHOLOGY FOR THE MATURATION OF NASCENT PARTICLE IN A TURBULENT LIFTED JET FLAME

by

Tingyu ZHAO*, Junhua FANG, and Zhen HUANG

Key Laboratory for Power Machinery and Engineering of M. O. E.,
Shanghai Jiao Tong University, Shanghai, China

Original scientific paper
https://doi.org/10.2298/TSCI211116057Z

In order to understand the soot formation in Diesel engine, a turbulent jet flame is used to simulate the combustion in the cylinder. The experimental study is performed to investigate the evolution of soot morphology for the maturation of nascent particle in a turbulent lifted jet flame fueled by n-heptane/toluene mixtures. An ultrasonic atomizer is used to evenly spread the fuel droplets to acquire single primary particles. Transmission electron microscopy is used to study the morphology of the particle sampled from the flame at different heights. Small soot aggregates are acquired from all the samples. Particle maturation such as agglomeration is accelerated under a high temperature by comparing the particle morphology sampled on the centerline and the wings of the flame. The precursors of nascent particles are depicted as dark nucleation dispersed to semitransparent polycyclic aromatic hydrocarbons. The nanostructure of nascent particles transforms from an amorphous state to an onion structure with the maturation of particles. Surface growth initially dominates the maturation of nascent particles in the direction of outside to inside for single particles. Agglomeration begins to emerge with the increased probability of collision at the end of maturation. Surface growth and agglomeration increase the mean particle diameter as the flame height increases. The oxidability of particles that undergo surface growth and agglomeration notably increases. The structure of nascent particles is inclined to be ordered and the mean particle diameter decreases with oxidation dominating the combustion reaction.

Key words*: soot morphology, transmission electron microscopy, nascent particles, jet flame*

Introduction

Soot is a major pollutant in many engineering systems, especially diesel engines [1, 2] with harmful health and environmental effects [3]. Soot particles are normally considered products formed by hydrocarbon fuels through incomplete combustion or pyrolysis. Soot formation and evolution is now generally accepted to consist of three processes: fuel pyrolysis and polycyclic aromatic hydrocarbons (PAH) formation, soot nucleation and nascent soot particle formation, and particle surface growth, agglomeration and oxidation [4-9]. The entire complex physical and chemical changes occur in a few milliseconds and involve a gas-phase reaction, a phase change reaction (gas to solid), and growth of solid particles [10, 11]. The size and morphology of nascent particles and mature particles reveal the transformation of PAH to solid soot

* Corresponding author, e-mail: zty1993@sjtu.edu.cn

aggregates which can be used to understand the soot evolution process [3, 12]. These two characteristics are widely used in previous studies for premixed flame and diffusion flame [12-14].

The autoignition of liquid fuels in a turbulent environment is a complex phenomenon that involves the interaction between turbulent and chemical kinetics in the cylinder of a Diesel engine [15]. In order to further study the formation of soot particles in Diesel engine, soot evolution during autoignition in partly premixed turbulent flow is used to simulate the soot evolution in the cylinder. During the process, a turbulent premixed flame and turbulent diffusion flame exist simultaneously. In recent studies, a Cabra flame burner has been used to study partly premixed turbulent combustion that occurs in diesel cylinder [16, 17]. A Cabra flame burner has controllable co-flow combustion, which can provide co-flow thermal atmosphere temperatures, and the temperature can be adjusted to be greater than the autoignition temperature of the selected fuel. Jet flame, which are called turbulent lifted jet flame in some researches, is surrounded by a co-flow atmosphere [18, 19]. The combustion product of co-flow is water, which has little influence on the combustion of jet flame. Pickett *et al.* [20] reported that the soot evolution is highly affected by the role of ignition in jet flame stabilization. Relevant experimental results have demonstrated that a Cabra flame burner can provide a stable turbulent flame, which offers a good platform for particle evolution of diesel engine [17, 21-23].

Thermophoretic sampling particles diagnostics (TSPD) can be used to absorb particles in flames to a grid for observation, which was first employed by Dobbins and Megaridis [24] in their study of a laminar co-flow ethane diffusion flame. Soot particles are driven thermophoretically to the probe and the lower probe temperature is able to freeze and quench the chemical reaction of soot particles to ensure the morphology of the particle sample is consistent with that at the moment of sampling [24]. The 2-D morphology images of soot particles from different locations inside the flame can be obtained with transmission electron microscope (TEM) image analysis, which can be divided into low resolution transmission electron microscopy (LRTEM) and high resolution transmission electron microscopy (HRTEM) according to the magnification factor. However, TEM images are not useful for analyzing liquid-like particles sampled from fuel-rich locations inside the flame [12]. Typically, the analysis of TEM images is used to reveal the morphological characteristics of a nascent soot particle and its maturity in current studies [13, 21, 25].

Flame temperature is a vital parameter in the study of particle evolution. For example, after passing through the threshold temperature for soot carbonization, *i.e.*, 1500 K, large liquid-like particles rapidly convert to fully developed aggregates consisting of mature primary particles according to the research of Kholghy *et al.* [22]. In the work of Lahaye *et al.* [26] PAH gradually form mature soot from liquid-like particles in high temperature regions. In laminar diffusion flame, particle morphology and the maturation process have visible differences in the centerline and wings of the flame [13, 21, 22]. This is mainly because flame temperature and its changing process are very different. The longest reaction and the minimum temperature gradient with flame height occur at the centerline of the flame, which results that the particle evolution has different characteristics with other regions. The centerline of the flame is the most representative region for research of particle evolution, which is widely applied in various particle studies [27-30].

In this paper, a Cabra burner is used to investigate the transition from liquid-like particles to solid soot particles during the process of diesel autoignition. Commercial diesel consists hundreds of hydrocarbons, thus, a mixture of n-heptane/toluene is selected as surrogate fuel because the simple binary mixture has similar properties to diesel [29, 30]. An ultrasonic atomizer is utilized to spread fuel droplets evenly in the air which can simulate the process of mixture of air and fuel in the cylinder. Thus, the scattered nanoparticles in the flame can show

the morphology evolution of nascent particles. The temperature, soot morphology and particle size distributions (PSD) in the turbulent lifted jet flame of n-heptane/toluene mixtures are investigated. The TSPD is adopted to take samples at specific flame heights in the centerline and wings of the flame. The TEM image analysis is used to study the morphology and size of the soot particle samples. The main goal of this study is to understand the formation of nanoparticles in diesel engine.

Experimental methodology

Burner and sampling system

Figure 1 shows the experimental burner and sampling system. A Cabra flame burner is employed to produce partially premixed turbulent lifted jet flame at low co-flow thermal atmosphere temperature for n-heptane, analytical reagent (AR), with a 10% volumetric addition of toluene (AR). In this study, the burner position is fixed, and the outer edge is a co-flow stainless ring with an outer diameter being of 222 mm. A copper jet tube is in the center of burner and has an outer diameter and wall thickness of 12 mm and 1 mm, respectively. The tube is 70 mm higher than the inner surface of the burner. A temperature-controllable thermo-atmosphere is provided by co-flow that is blown steadily around the tube with an air/hydrogen mixture. The flame and flow conditions are shown in tab. 1. The hydrogen and air-flow rate are 1000 slm (at 293 K) and 126 slm (at 293 K), respectively. The co-flow is oxygen-enriched combustion with an *F*/*A* ratio of 0.3. The experimental thermo-atmospheric temperature is approximately 568 K, which is greater than the autoignition temperature of n-heptane. Thus, the spontaneous combustion of fuel can occur.

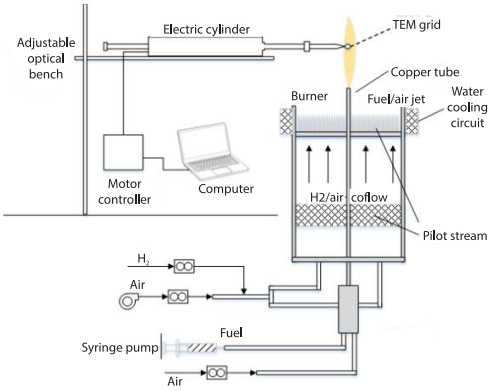

Figure 1. Cabra burner and thermophoretic soot sampling system

Table 1. Flame and flow conditions

Coflow		Central jet	
Q_{H2} [slm]	126	Q_{fuel} [ml per hour]	80
Q_{air} [slm]	1000	Q_{air} [slm]	10
T_{coflow} [K]	568	T_{jet} [K]	273
D_{coflow} [mm]	2222	D_{jet} [mm]	12
F/*A* ratio	0.3	*F*/*A* ratio	≈0.6

Fuel is constantly supplied by a springe pump at a constant flow rate of 80 ml per hour. Before entering the jet tube, the fuel is ultrasonic atomized to become relatively well-dispersed small droplets with a high concentration. The atomized droplets are mixed with air at a flow rate of 10 slm (at 273 K) to move to the jet tube outlet. The frequency of the ultrasonic atomizer is 120 kHz. The diameter of the fuel droplets is approximately 12.73 μm according to eq. (1) [31], which is similar to the size of diesel droplet in the cylinder [32]. Examples of centered formulas:

$$D = 0.34\left[\frac{8\pi T}{\rho f^2}\right]^{1/3} \tag{1}$$

where D is the mean diameter of fuel, T – the surface tension coefficient of liquid, ρ – the fuel density, and f – the ultrasonic frequency.

The sample grid is held by stainless steel self-closing tweezer with probe dimensions of 0.10×0.06 mm, which is fixed on a linear electric cylinder (Parker EET032, USA. A linear electric cylinder provides accurate reciprocal motion with computer control to ensure an exact grid position in the horizontal direction and proper exposure time inside the flame. The exposure time is set to 10 ms for appropriate grid coverage [24, 27]. Less transit time and suitable exposure time are able to protect the grid from thermal damage. The linear electric cylinder is fixed on an adjustable optical bench, and the sampling height is regulated using a platform on the optical bench. The top of the jet tube is selected as the reference for flame height ($HAB = 0$).

Temperature measurements

The temperature measurement locations are similar to the sampling positions. Temperature measurements are performed with a 50 μm uncoated *R*-type thermocouple (Pt/13%Rh-Pt) [28], and the data are input to a computer via a capture card. The thermocouple is tightened and fixed on the linear electric cylinder and then rapidly inserted into the flame for measurement, which may decrease particle deposition for reducing measurement error [33]. According to previous studies, measurement error may be produced by the thermocouple in the flame due to particle deposition, heat conduction, surface reaction, thermal radiation and other factors [34-36]. In the study, temperature is corrected based on relative methods documented in the research of Botero *et al*. [37].

The TEM images and image analysis

Carbon-supported grids (300 mesh) and holey carbon film grids (300 mesh) are used to collect soot particles. The former is used for general morphology research, and the latter is used for nanostructure research. The TEM images are taken by an FEI Talos F200X microscopy at an accelerating voltage of 200 kV. At least ten images are taken for different grids of a sample. The magnification factor for LRTEM images is 36000 while the magnification factor for HRTEM images is 1.05 M. Image Pro Plus (IPP) is used to analyze the TEM images [38, 39]. For LRTEM images, the size of single particle is defined as the average value of the smallest diameter and the largest diameter of a particle. 100 well-dispersed particles of the same sample in different grids are selected randomly to measure the average particle diameter. The processing procedure for HRTEM images is to select an image region; then, in terms of Fourier transform, frequency filter, inverse Fourier transform, binary conversion and skeletonization are conducted for images using IPP. The fringe separation distance and fringe length may be determined from the data acquired from the processed image according to IPP [38].

Results and discussion

Evolution of soot morphology

Figure 2 shows the morphology of particles at various heights along the centerline and wings. Figures 2(a)-2(f)represents the process of liquid-like particle transition solid particles in the centerline. Figure 2(a) and 2(b) shows the generation of nascent particles. There is a clear semitransparent area in fig. 2(a), in which dark nucleation area of various sizes are scattered. These particles are obviously larger than the surrounding single particles. In fig. 2(b), the particles are scattered evenly, and their diameters are significantly larger than those in fig. 2(a). Furthermore, these particles do not have a uniform shape and have some differences in diameter. There is also no semitransparent area. All the particles in this process are nascent soot particles,

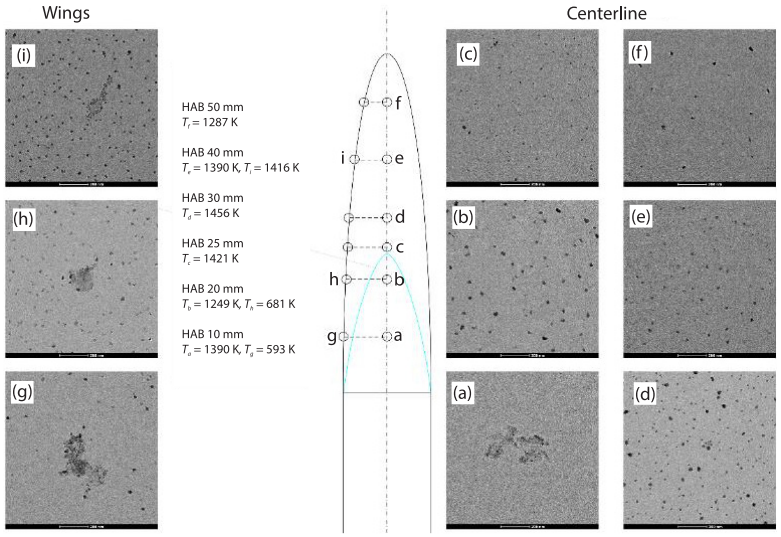

Figure 2. The TEM pictures (36000×) of samples from different heights in the centerline (a) and wings (b) of the flame

and are converted from PAH which are produced by combustion. Moreover, the formation and growth of PAH involves transformation from the gas phase to solid phase. At the initial stage of PAH formation, the main substances exist in a gas or liquid phase, which are shown as semitransparent areas in the TEM images. PAH is the critical nutrient for particle growth. Thus, Nascent particle size increases as the intermediate product PAH content decreases.

The maturation process of the initial soot particles is illustrated from figs. 2(b)-2(f). In terms of morphology, the particles in fig. 2(c) approach those in fig. 2(b), and thus the former is similar to the overall reduction in the latter. The particle shapes are irregular flat, and the major difference between the particles is size. Compared to nascent particles, the more mature particles show more layering and are closer to globularity or ellipsoid, as shown in fig. 2(d). In addition, there are some obvious large particles in fig. 2(d). Areas of these particles are darker in color and more layered than other areas due to agglomeration. In fig. 2(e), particles are manifested as the product generated by agglomeration after collision with each other, so their appearance are not ellipsoid. There are two areas for the produced particles after agglomeration, *i.e.*, the area where numerous particles are overlapped and the area where they do not overlap. Large aggregate solid particles are not expected to appear, and the particle sizes are slightly smaller than the large particles in fig. 2(d). Particle density decreases significantly from figs. 2(d) and 2(e), which also shows the mutual collision of particles has increased. Particles after the collision of different areas exerts various natures in oxidability. In this case, the difference of collision angle and the size of the agglomeration area result in the larger morphology differences and diameter fluctuations among the soot particles with the development of the combustion process. This phenomenon is apparent in fig. 2(f), in which there are larger morphology differences with a smaller particle density among particles.

Figures 2(g)-2(i) show the particle morphology at several typical positions of the wings. Compared with samples along the centerline at the same height, particles collected from the wings have some irregular semitransparent areas, which indicates that there are still numerous particle precursors at every moment on the wings. This finding may be due to more dispersed fuel droplets with larger diameter in certain fringe areas of the jet spray. In this case,

a short period of violent combustion could occur in these areas, which produces plenty of PAH. Instability of turbulent diffusion combustion is more evident in these areas.

For figs. 2(a) and 2(g), the morphology distributions are extremely similar and manifest as a large semitransparent area with a small number of single particles scattered. The particle size in fig. 2(g) is remarkably greater than that in fig. 2(a). The main reason for this phenomenon might be the difference in flame temperature. The temperature in the axis area was approximately 200 K greater than in the fringe area at the same height. Particles of new nucleation are smaller in hot environments. Particles in fig. 2(b) and 2(h) are also similar to each other in terms of morphology. However, the temperature of the sampling area is higher in fig. 2(b), and the particle size is slightly larger than that in fig. 2(h). This is because the fuel density, which is obviously greater at the centerline than at the wings, offers more PAH for particle growth. Comparing fig. 2(e) with 2(i), the flame temperature at the wings is slightly less than the centerline temperature and the particles in both areas are ellipsoids. The difference is that agglomeration occurs at the centerline, but this phenomenon is not clear at the wings. Particle motion may be accelerated by higher temperature. Moreover, the particle density at the centerline is higher, which results that collisions with each other are more possible.

The differences in the evolution of flame temperature and particle morphology at the centerline and wings shows that temperature is an inherent motive force for particle evolution. High temperature may enhance particle oxidative activity, which results in similar sized particles. Some reactions can only occur when the temperature reaches a certain value. According to previous research, there is a threshold temperature for soot carbonization at 1500 K [22]. In selected conditions, large solid aggregate particles are not collected in the samples because the maximum flame temperature is less than 1500 K. Furthermore, fuel distribution has an important influence on particle maturation. An area with large fuel density can provide more PAH for particle generation and growth, which increases collision probability among particles.

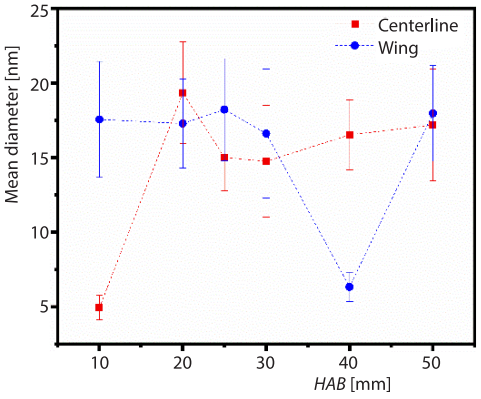

Figure 3. Average particle diameter at different heights along the centerline

Particle size distributions on the centerline of the flame

Figure 3 shows the variation of average particle diameter with height for particles along the centerline. The variation of average particle diameter is increase, followed by a decrease and increase again. The variation can be divided into two-stages based on morphology evolution. From $HAB = 10$ mm to $HAB = 20$ mm, PAH nucleation and the formation of nascent particles occurs. Nascent particles absorb free PAH for surface growth, so the particle size increased distinctly. From $HAB = 20$ mm to $HAB = 50$ mm, the particle maturation process is carried out. There are multiple processes involved in particle maturation such as surface growth, oxidation and agglomeration. The PAH content would decrease at higher temperature. In this case, oxidation has the dominant position so particle size decreases gradually with height. Oxidized particles increased in order while their oxidability decreased. The decrease in particle diameter is weakening and the particles size slowly increases with the increase in mutual collisions. For particles with higher maturity before being aggregated, their average diameter would be closer.

Figure 4 shows histograms of the PSD for each stage of maturation. The PSD directly embodies the impact of various factors on particle evolution. At *HAB* = 20 mm, particle size is similar to normal distribution, which is the required distribution for fully-formed nascent particles. However, the particle size is concentrated approximately 10-14 nm with over 60% of the particles in this range at *HAB* = 25 mm. There is not a particle with diameter greater than 22 nm, which indicates that the particle size decreased under the domination of oxidation. Here, large particles are especially affected by oxidation. At *HAB* = 30 mm, the particle size distribution is more focused than the previous distribution, nearly 70% particles are distributed in the range of 12-16 nm. Moreover, some particles have diameters between 20-30 mm. The sizes of some particles are approximately double the most common particle sizes, which demonstrate that the large particles are generated by small particle agglomeration combined with morphology. Comparing the size distribution of *HAB* = 25 mm and *HAB* = 30 mm, the particle size is significantly influenced by oxidation. When the particle size is reduced to a certain degree, the maturation of particles is no longer dominated by oxidation, as the PSD is focused on a certain area with less variation. At *HAB* = 40 mm, the distribution size gradually approaches that of a normal distribution. Particle sizes are not concentrated on a narrow interval without the appearance of large particles, indicating that agglomeration has basically completed and the large particles are obviously affected by oxidation. The variation of size distribution in the entire process embodies the impact of oxidation and agglomeration on the maturation of nascent soot particles.

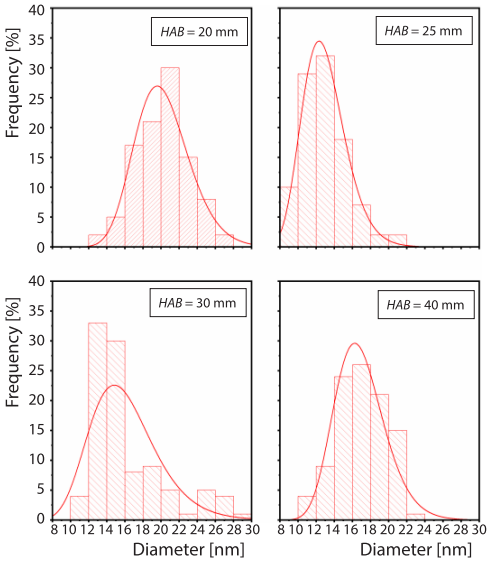

Figure 4. Histograms of the PSDFS for samples at different heights along the centerline

Evolution of nanostructure on the centerline of flame

Figure 5 shows the HRTEM images of particles at different flame heights while fig. 6 shows the variation of mean fringe length and fringe separation distance with flame height calculated with IPP. Overall, the mean fringe separation is obviously larger than that of graphitic carbon (approximately 0.335 nm), which also suggests that complete carbonization does not occur under the experimental conditions. Fringe length increases and the micro-structure becomes compact and orderly with the development of the combustion processes.

Figure 7 shows the frequency distribution of fringe separation distance. There is a distinct characteristic when comparing fringe separation distance distribution for particles at different heights. With the increase in flame height, the large fringe separation distances that approach 0.5 nm decrease significantly, while the fringe separation distances close to graphitic carbon start to appear.

Combining figs. 5 and 7, there is no recognizable fringes in fig. 5(a) and its nanostructure presents on amorphous state. As mentioned before, these particles belong to nascent particles. The onion structure starts to appear for particles from outside to inside in fig. 5(b) and the fringe separation distance decreases gradually in the same direction. The mean fringe

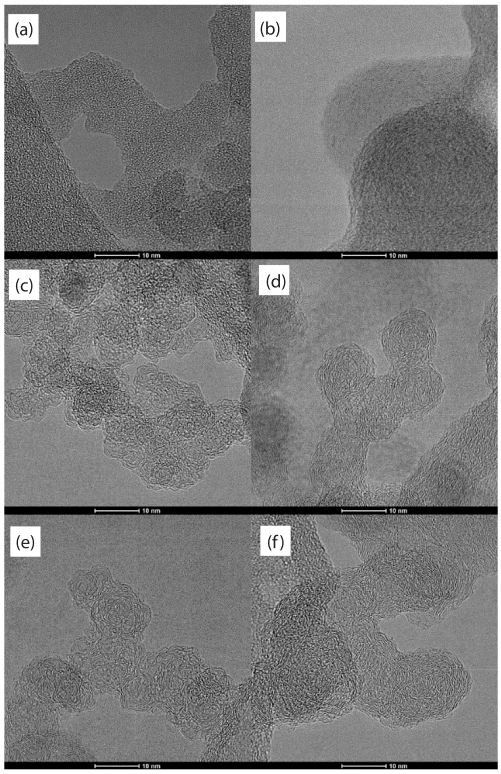

Figure 5. The HRTEM pictures (1.05M×) of particles at different flame heights along the centerline; (a) *HAB* = 10 mm, (b) *HAB* = 20 mm, (c) *HAB* = 25 mm, (d) *HAB* = 30 mm, (e) *HAB* = 40mm, and (f) *HAB* = 50 mm

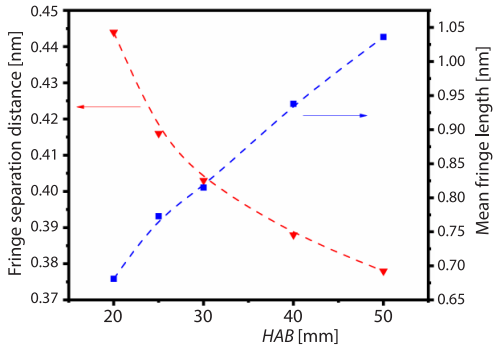

Figure 6. Mean fringe length and fringe separation distance for samples at different heights along the centerline

separation distance is much larger than that of graphitic carbon, which indicates the particle maturity is low. Moreover, the mean fringe separation distance for particles in fig. 5(c) further decreases with the combustion process. The distribution is more extensive and there is a greater difference between the fringe separation distances for particles of various areas. Particles are also in varying order at this height. Particle surface growth promotes the maturation of soot particles via a series of physical and chemical processes on surface of nascent soot particles.

Comparing figs. 5(a)-5(c), the particles transform from a disordered amorphous structure to an ordered onion structure, and the growth direction is from outside to inside. The direction of newly generated microcrystalline is in a state of chaos without a clear center and the fringe separation distance distribution has large fluctuations. It because that the reactivity and reaction speed of surface growth for particles are different in different areas due to environmental asymmetry. A messy micro-structure at the particle edges and a large fringe separation distance are beneficial for oxidation. However, with oxidation of the edges and disordered microcrystalline layer, an obvious center begins to emerge at the microcrystalline layer. Growth and merging occur among the fringes so the length of fringe increases, which is shown from figs. 5(c) and 5(d). There is a microcrystalline layer in different directions in fig. 5(c), which is especially reflected in the edges of particles. The particle shape is closer to globularity and the microcrystalline layer is uniformly distributed along the center of the sphere in fig. 5(d). The mean fringe separation distances for both are 0.773 nm and 0.815 nm, respectively, but there is an obvious increase for the latter figure. With the progress of collision, the morphology of soot particles with onion structure in fig. 5(e) and 5(f) transitions from a single core to multicore, and the latter microcrystalline layer is more orderly than the former, which may be due to particle agglomeration. The agglomeration is the process of collision growth for the particles. With the increase in matured particles, the probability of collision increases accordingly. The arrangement of fringes at the edge of

newly collided particles are destroyed, which promote the development of oxidization. These particles gradually become larger solid agglomerated particles after the irregular fringes being oxidized.

From the aforementioned description, surface growth and agglomeration play vital role in particle growth in the process of particle maturation, which is mainly determined by external factors. Surface growth requires free radical and active molecules which should exist in the flame, so it is mainly controlled by flame status. In contrast, agglomeration is affected by the number and space distribution of particles, which is primarily found at the end of combustion. Furthermore, surface growth and agglomeration are both beneficial for size growth. Particle oxidation not only depends on burning status, but also relies on surface growth and agglomeration. They may disorder the micro-structure at the edge of particles, and oxidative activity may increase, which enhances oxidability from another perspective. Oxidation promotes the decrease in particle size, which is beneficial for merging and growth among fringes in the nanostructure.

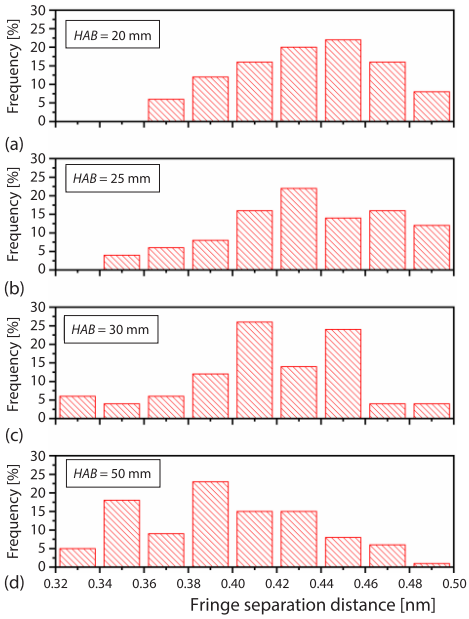

Figure 7. Frequency distribution of fringe separation distance for samples at different heights along the centerline

Conclusions

The study mainly focuses on the evolution of particle morphology and size in transition of liquid-like particles to solid soot particles to understand the soot formation in the diesel engine. The specific conclusions are as follows.

- Flame temperature is the driving force for particle maturation, which has a significant effect on particle oxidation. Particle maturation is accelerated under high temperature, as both complete generation of nascent particles and carbonization have to reach a certain temperature.
- Nascent soot particulates are transferred from PAH, and their nanostructure presents on amorphous state. As the particle micro-structure becomes ordered, the morphology of the particles tends to be globular or ellipsoid. The collision of particles leads to morphologic differentiation for single mature particles.
- During the series process of soot nucleation and the formation of nascent particles, surface growth mainly continues from outside to inside and the mean size increases accordingly. With the development of the reaction, the reactivity of the surface increases, and particle oxidability increases, whereas the mean size gradually decreases. As particles are mostly oxidized, a more ordered micro-structure is formed. As a result, particle oxidation is diminished, and the probability of collision increases. Then, the agglomeration of particles begins to emerge. Finally, the mean size increases again. The oxidability of particles after collision strengthens and the increase in the particle size slows.
- The formation of carbonaceous soot must reach the threshold temperature and long combustion duration. Thereby, the diesel engine can reduce carbonaceous soot particles with the low temperature combustion mode and rapid combustion.

Acknowledgment

This work was financially supported by National Natural Science Foundation of China (51376117).

References

[1] Muller, J. O., *et al.*, Diesel Engine Exhaust Emission: Oxidative Behavior and Microstructure of Black Smoke Soot Particulate, *Environmental Science & Technology*, *40* (2006), 4, pp. 1231-1236
[2] Xiao, H., *et al.*, An Experimental Study of the Combustion and Emission Performances of 2, 5-dimethylfuran Diesel Blends on a Diesel Engine, *Thermal Science*, *21* (2017), 1B, pp.543-553
[3] Kim, W., *et al.*, Soot Aggregates, Superaggregates and Gel-Like Networks in Laminar Diffusion Flames, *Journal of Aerosol Science*, *37* (2006), 3, pp. 386-401
[4] Dobbins, R. A., Hydrocarbon Nanoparticles Formed in Flames and Diesel Engines, *Aerosol Science and Technology*, *41* (2007), 5, pp. 485-496
[5] Frenklach, M., Reaction Mechanism of Soot Formation in Flames, *Physical Chemistry Chemical Physics*, *4* (2002), 11, pp. 2028-2037
[6] Glassman, I., Soot Formation in Combustion Processes, in: Symposium (International) on Combustion, *Elsevier*, *22* (1988), 1, pp. 295-311
[7] Morgan, N., *et al*., Numerical Simulations of Soot Aggregation in Premixed Laminar Flames, *Proceedings of the Combustion Institute*, *31* (2007), 1, pp. 693-700
[8] Wang, H., Formation of Nascent Soot and Other Condensed-Phase Materials in Flames, *Proceedings of the Combustion Institute*, *33* (2011), 1, pp. 41-67
[9] Ju, H., *et al*., Modelling of Soot Particle Collision and Growth Paths in Gas-Solid Two-Phase Flow, *Thermal Science*, *25* (2021), 5B, pp. 3741-3752
[10] Cain, J. P., *et al*., Micro-FTIR Study of Soot Chemical Composition – Evidence of Aliphatic Hydrocarbons on Nascent Soot Surfaces, *Physical Chemistry Chemical Physics*, *12* (2010), 20, pp. 5206-5218
[11] D'Anna, A., Combustion-Formed Nanoparticles, *Proceedings of the Combustion Institute*, *32* (2009), 1, pp. 593-613
[12] Tian, K., *et al*., Determination of the Morphology of Soot Aggregates Using the Relative Optical Density Method for the Analysis of TEM Images, *Combustion and Flame*, *144* (2006), 4, pp. 782-791
[13] Kempema, N. J., *et al.*, Combined Optical and TEM Investigations for a Detailed Characterization of Soot Aggregate Properties in a Laminar Coflow Diffusion Flame, *Combustion and Flame*, *164* (2016), Feb., pp. 373-385
[14] Tang, Q., *et al*., Soot Formation Characteristics of n-Heptane/Toluene Mixtures in Laminar Premixed Burner-Stabilized Stagnation Flames, *Combustion and Flame*, *187* (2018), Jan., pp. 239-246
[15] Mastorakos, E., Ignition of Turbulent non-Premixed Flames, *Progress in Energy and Combustion Science*, *35* (2009), 1, pp. 57-97
[16] Cabra, R., *et al*., Simultaneous Laser Raman-Rayleigh-LIF Measurements and Numerical Modelling Results of a Lifted Turbulent H_2/N_2 Jet Flame in a Vitiated Coflow, *Proceedings of the Combustion Institute*, *29* (2002), 2, pp. 1881-1888
[17] Cabra, R., *et al.*, Lifted Methane-Air Jet Flames in a Citiated coflow, *Combustion and Flame*, *143* (2005), 4, pp. 491-506
[18] Cabra, R., *Turbulent Jet Flames into a Vitiated Coflow*, University of California, Berkeley, Cal., USA, 2003
[19] Xie, K., *et al*., Experimental Study on the Effect of Spray Cone Angle on the Characteristics of Horizontal jet Spray Flame under Sub-Atmospheric Pressure, *Thermal Science*, *24* (2020), 5A, pp. 2941-2952
[20] Pickett, L. M., Low Flame Temperature Limits for Mixing-Controlled Diesel Combustion, *Proceedings of the Combustion Institute*, *30* (2005), 2, pp. 2727-2735
[21] Kholghy, M. R., The Evolution of Soot Morphology in Laminar co-Flow Diffusion Flames of the Surrogates for Jet A-1 and a Synthetic Kerosene, Ph. D. thesis, University of Toron, Toron, Canada, 2012
[22] Kholghy, M., *et al*., The Evolution of Soot Morphology in a Laminar Coflow Diffusion Flame of a Surrogate for Jet A-1, *Combustion and Flame*, *160* (2013), 10, pp. 2119-2130
[23] Myhrvold, T., *et al*., A Numerical Investigation of a Lifted H_2/N_2 Turbulent Jet Flame in a Vitiated Coflow, *Combustion Science and Technology*, *178* (2006), 6, pp. 1001-1030
[24] Dobbins, R. A., *et al*., Morphology of Flame-Generated Soot as Determined by Thermophoretic Sampling, *Langmuir*, *3* (1987), 2, pp. 254-259

[25] Williams, T. C., *et al.*, Measurement of the Dimensionless Extinction Coefficient of Soot Within Laminar Diffusion Flames, *International Journal of Heat and Mass Transfer*, *50* (2007), 7-8, pp. 1616-1630
[26] Lahaye, J., *et al.*, Mechanisms of Carbon Black Formation, *Correlation with the Morphology of Aggregates Carbon*, *32* (1994), 7, pp. 1319-1324
[27] Botero, M. L., *et al*., The HRTEM Evaluation of Soot Particles Produced by the Non-Premixed Combustion of Liquid Fuels, *Carbon*, *96* (2016), Jan., pp. 459-473
[28] Botero, M. L., *et al.*, Sooting Tendency and Particle Size Distributions of n-Heptane/Toluene Mixtures Burned in a Wick-Fed Diffusion Flame, Fuel, *169* (2016), Apr., pp. 111-119
[29] Saffaripour, M., *et al*., A Numerical and Experimental Study of Soot Formation in a Laminar Coflow Diffusion Flame of a Jet A-1 Surrogate, *Proceedings of the Combustion Institute*, *34* (2013),1, pp. 1057-1065
[30] Seong, H. J., *et al.*, Studies of Soot Oxidative Reactivity Using a Diffusion Flame Burner, *Combustion and Flame*, *159* (2012), 5, pp. 1864-1875
[31] Lang, R. J., Ultrasonic Atomization of Liquids, The Journal of the Acoustical Society of America, *34* (1962), 1, pp. 6-8
[32] Wang, X., *et al*., Experimental and Analytical Study on Biodiesel and Diesel Spray Characteristics under Ultra-High Injection Pressure, *International Journal of Heat and Fluid-Flow*, *31* (2010), 4, pp. 659-666
[33] Cundy, V. A., *et al.*, Constant-Tension Thermocouple Rake Suitable for use in Flame Mode Combustion Studies, *Review of Scientific Instruments*, *57* (1986), 6, pp. 1209-1210
[34] Bergman, T. L., *et al.*, *Fundamentals of Heat and Mass Transfer*, John Wiley & Sons, New York, USA, 2011
[35] McEnally, C. S., *et al*., Soot Volume Fraction and Temperature Measurements in Laminar non-Premixed Flames Using Thermocouples, *Combustion and Flame*, *109* (1997), 4, pp. 701-720
[36] Shaddix, C. R., Correcting Thermocouple Measurements for Radiation Loss: A Critical Review, *Proceedings*, 33rd Nat. Heat Tran. Conf., Albuquerque, N. Mex., USA, 1999
[37] Botero, M. L., *et al.*, Sooting Tendency of Surrogates for the Aromatic Fractions of Diesel and Gasoline in a Wick-Fed Diffusion Flame, *Fuel*, *153* (2015), Aug., pp. 31-39
[38] Shim, H., *et al*., A for Analysis of 002 Lattice Fringe Images and Its Application Combustion-Derived Carbons, *Carbon*, *38* (2000), 1, pp. 29-45
[39] Vander W., *et al*., Analysis of HRTEM Images for Carbon Nanostructure Quantification, *Journal of Nanoparticle Research*, *6* (2004), 6, pp. 555-568

Paper submitted: November 16, 2021
Paper revised: March 30, 2022
Paper accepted: April 4, 2022